Steel and Composite Structures, *Vol. 29, No. 4 (2018) 423-435*
DOI: https://doi.org/10.12989/scs.2018.29.4.423

Effect of creep on behaviour of steel structural assemblies in fires

Peter Češarek [1a], Miha Kramar [2b] and Jerneja Kolšek [*3]

[1] *University of Ljubljana, Faculty of Civil and Geodetic Engineering, Jamova 2, SI-1000, Ljubljana, Slovenia*
[2] *ZAG - Slovenian National building and Civil Engineering Institute, Section for Metal, Timber and Polymeric Structures, Dimičeva 12, SI-1000 Ljubljana, Slovenia*
[3] *ZAG - Slovenian National building and Civil Engineering Institute, Fire Laboratory and Fire Engineering, Dimičeva 12, SI-1000 Ljubljana, Slovenia*

(*Received December 3, 2017, Revised July 5, 2018, Accepted September 19, 2018*)

Abstract. There are presently two general ways of accounting for hazardous metal creep in structural fire analyses: either we incorporate creep strains implicitly in hardening model ('implicit-creep' plasticity) or we account for creep explicitly ('explicit-creep' plasticity). The first approach is simpler and usually used for fast engineering applications, e.g., following proposals of EN 1993-1-2. Prioritizing this approach without consideration of its limitations, however, may lead to significant error. So far the possible levels of such error have been demonstrated by few researchers for individual structural elements (i.e., beams and columns). This paper, however, presents analyses also for selected beam-girder assemblies. Special numerical models are developed correspondingly and they are validated and verified. Their important novelty is that they do not only account for creep in individual members but also for creep in between-member connections. The paper finally shows that outside the declared applicability limits of the implicit-creep plasticity models, the failure times predicted by the applied alternative explicit-creep models can be as much as 40% shorter. Within the limits, however, the discrepancies might be negligible for majority of cases with the exception of about 20% discrepancies found in one analysed example.

Keywords: steel structures; fire; creep; fin plate connections; restrained beams

1. Introduction

Metal creep is time-dependent plastic strain under constant stress which occurs due to movement of dislocations in the slip plane and accelerates with increase in temperature (Kodur and Dwaikat 2010). There has been a growing belief among researchers on creep having a significant in influence on the mechanical response of steel structures in fire, e.g., Anderberg (1988). Thus, it has been generally agreed that a correct mathematical description of fire response should explicitly consider three strain components: (i) thermal strains, (ii) mechanical strains and (iii) creep strains. However, so as to simplify the calculations for practical fire engineering purposes, only the first two strain components are often considered, e.g., such as in the approach proposed in EN 1993-1-2 (2004), in Chan *et al.* (2010), in Torić *et al.* (2013) or in (2016a) while the creep strains are incorporated indirectly in the stress-mechanical strain relationship (i.e., implicit-creep stress-mechanical strain relationship). Nevertheless, as discussed already by other researchers (e.g., Anderberg 1988, Torić *et al.* 2016a, Kodur *et al.* 2010), while such approaches are accurate enough for some cases they could be too approximate for others as the real temperature and stress history cannot always be accounted for satisfactorily in this way and for every possible practical scenario.

Anderberg (1988) was one of the first who investigated the effect of creep on fire response of small-scale simply-supported beams and confirmed a noticeable influence. In his work, he also expressed a suspicion that 'for fire-exposed slender steel columns, the influence of creep' could 'be even further pronounced'. Later on, Huang *et al.* (2006) and Torić *et al.* (2016a) were led to the same conclusions while exploring the influence of creep on buckling of steel columns numerically at different heating rates and boundary restraints. A similar-type of a study was also presented by Li and Zhang (2012). Experimental proof about the effect of creep on buckling of steel columns was presented by Yang and Yua (2013). Furthermore, for similar reasons as for cases of columns, a pronounced effect of creep is to be expected also with restrained beams since these can survive higher temperatures due to the effect of axial restraint (thus, creep strains can evolve to a greater extent). This has been shown recently, e.g., in Torić *et al.* (2015), in Kodur and Dwaikat (2010) and Kodur *et al.* (2010) where different creep models (including a new one proposed by the authors themselves) were explored at different degrees of end-restraint of the beam, various load levels, and heating regimes. In addition, in realistic fire scenarios (often called 'natural fires'), which are discussed more and more in recent literature, the structure can be exposed to moderately high temperatures (i.e., 500°C - 700°C) for a long period of time what also makes the structural conditions favourable for more pronounced creep deformations to evolve.

*Corresponding author, Ph.D.,
E-mail: jerneja.kolsek@zag.si
[a] Ph.D.
[b] Ph.D.

ISSN: 1229-9367 (Print), 1598-6233 (Online)

Regardless of the fact that the belief about the great importance of creep on fire response of steel structures had been present for a long time, the low number of the corresponding investigations as available at present clearly indicates that so far this problem has not received enough attention. In addition, individual structural members (i.e., isolated from adjacent structure) have been investigated so far. However, results from analyses of structural assemblies, which could also demonstrate the effect of creep in between-member connections, are not yet available. Furthermore, investigations comparing the explicit-creep models against alternative implicit-creep plasticity approaches (such as, e.g., Kodur and Dwaikat 2010, Kodur *et al*. 2010, Anderberg 1988, Li and Zhang 2012, Torić *et al*. 2016a) are rare as well.

The fundamental aim of this paper is an investigation of the effects of creep and a comparison of implicit-creep and explicit-creep plasticity approach in modelling response of steel structural assemblies exposed to fires. The investigation is done by means of a specially designed parametric study (Sections 2.4.2 and 3). For purposes of the parametric study, a model of a typical assembly of a steel beam at each end connected to a steel girder with a bolted shear end-plate connection is prepared and presented in details (Sections 2.1 and 2.2) as well as suitably verified and validated (Section 2.3). The study comprises several numerical analyses performed at two heating rates; the first one corresponding to the lower limit of applicability of the selected implicit-creep plasticity model and the second one corresponding to a rate below this limit. The aim of comparing both creep modelling approaches also at the second rate is to explore possible consequences when the usage of the implicit-creep model is inappropriately stretched to heating regimes below the allowable lower limit (e.g., such as for simulations of steady-state fire phase of real fires) what is often observed in the engineering practice.

2. The model

This section presents the two-step finite-element model which was prepared for analyses of a selected steel beam-girder structural assembly (Sections 2.1-2.2) using the FEMA computing environment ABAQUS (2016). For geometrical FE discretizations and for thermal descriptions of materials the built-in tools were used. Suitable algorithms were implemented in the model using the user subroutine UMAT, for mechanical (stress-strain) descriptions of materials. A scheme of the assembly is shown in Fig. 1. Conveniently the characteristics of this assembly follow closely the characteristics of the assembly tested in the well-known Cardington fire experiment Wald *et al*. (2006), which we used for model validation. Nevertheless, the model presented in this paper and its results can be easily applied also to other cases with similar geometries.

2.1 Thermal response analysis (1st step)

The first (thermal) step of the analysis is set to be performed as a standard Fourier's heat conduction analysis.

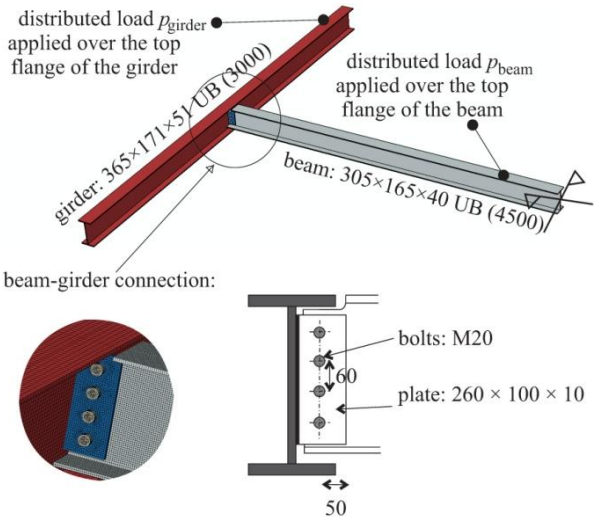

Fig. 1 Scheme of the analysed structural assembly (only one girder and a half of the beam is modelled considering the symmetry of the geometry). The additional denotations of the girder and the beam (enclosed) in brackets, represent the length of the girder or a half of the length of the beam, respectively. All dimensions are in millimetres

The type of finite elements used is DC3D8. Thermal properties of steel and their temperature dependence are taken as proposed in EN 1993-1-2 (2004).

2.2 Analysis of structural response (2nd step)

For mechanical part of the analysis, the geometrical details of the individual parts and the assembly are taken from the first step of the analysis but they are now discretized by C3D8 finite elements. In addition to mechanical loading, the time-dependent temperatures of the elements' nodes, calculated in the preceded thermal analysis, are imported to impose thermal load. Moreover, surface to surface contact interactions with finite sliding formulation are assigned to surfaces of the beam-girder connection that are in contact initially (the web of the beam and the end plate) or could be put into contact during deformation (bolts and plates, the flange of the beam and the girder). For computations the implicit solver and the general static analysis are engaged.

2.2.1 Material models

The theoretical frame of material models is the well-known 'principle of additivity of strains'. Correspondingly, as explained e.g., in Anderberg (1988), the total (often called 'geometrical') strain tensor $\boldsymbol{\varepsilon}^k$ (upper-script k denotes time station t^k) in a generic particle of the body is first decoupled to the given tensors of stress and strains at time t^{k-1} and the known temperatures at $t^k > t^{k-1}$ and t^{k-1}

$$\boldsymbol{\varepsilon}^k = \boldsymbol{\varepsilon}^{k-1} + \Delta\boldsymbol{\varepsilon}^k. \quad (1)$$

In Eq. (1) $\Delta\boldsymbol{\varepsilon}^k$ is the increment of the total (i.e., geometrical) strain tensor in the time interval $[t^{k-1}, t^k]$.

This is decoupled further as the sum of the strain increments due to change of: (i) temperature, $\Delta\boldsymbol{\varepsilon}_{th}^{k}$ and (ii) stress, where the stress-induced parts are of two types: time-independent mechanical strains $\Delta\boldsymbol{\varepsilon}_{\sigma}^{k}$, and time-dependent creep strains, $\Delta\boldsymbol{\varepsilon}_{cr}^{k}$

$$\Delta\boldsymbol{\varepsilon}^{k} = \Delta\boldsymbol{\varepsilon}_{th}^{k} + \Delta\boldsymbol{\varepsilon}_{\sigma}^{k} + \Delta\boldsymbol{\varepsilon}_{cr}^{k}. \tag{2}$$

Here it is assumed that models describing the stress-strain relationship can be found separately and independently for each strain component. As a simplification of Eq. (2), an alternative approach is used sometimes, e.g., such as proposed in EN 1993-1-2 (2004), Torić *et al*. (2013) or (2015), where creep strain is in an approximate way implicitly incorporated in the time independent stress – (mechanical) strain relationship. In this case, the total strain decomposition reads

$$\Delta\boldsymbol{\varepsilon}^{k} = \Delta\boldsymbol{\varepsilon}_{th}^{k} + \Delta\boldsymbol{\varepsilon}_{\sigma,imp-cr}^{k}. \tag{3}$$

In Eqs. (2) and (3) the mechanical strain increment also splits to its elastic and plastic part

$$\begin{aligned} \Delta\boldsymbol{\varepsilon}_{\sigma}^{k} &= \Delta\boldsymbol{\varepsilon}_{\sigma,e}^{k} + \Delta\boldsymbol{\varepsilon}_{\sigma,p}^{k} \\ \Delta\boldsymbol{\varepsilon}_{\sigma,imp-cr}^{k} &= \Delta\boldsymbol{\varepsilon}_{\sigma,e}^{k} + \Delta\boldsymbol{\varepsilon}_{\sigma,imp-cr,p}^{k}, \end{aligned} \tag{4}$$

where the elastic part is being considered as fully reversible and the inelastic part represents irreversible deformation. The creep strains $\Delta\boldsymbol{\varepsilon}_{cr}^{k}$, are assumed to be entirely irreversible too.

2.2.2 Thermal strains

Thermal strains in steel at time station t^{k} follow the assumption of an isotropic extension

$$\Delta\boldsymbol{\varepsilon}_{th}^{k} = \Delta\varepsilon_{th}^{k}\boldsymbol{I} = \alpha_{T}\Delta T\boldsymbol{I}, \tag{5}$$

where $\boldsymbol{I}$ is a unit tensor (a change in temperature will only cause deformation in normal direction) and α_{T} is temperature-dependent unidirectional extension coefficient, which is considered independent on the type of steel and is calculated as proposed in EN 1993-1-2 (2004).

2.2.3 Mechanical strains

The classic Mises' plasticity model with isotropic hardening is engaged in this paper for consideration of mechanical strains (Simo and Hughes 1998). The corresponding equations are discretized by applying implicit Euler scheme and solved by means of well-known return mapping algorithm, which returns the admissible stresses and corresponding values of plastic strains

$$\begin{aligned} \Delta\varepsilon_{\sigma,p}^{k} &= \sqrt{\frac{2}{3}}\Delta\lambda_{p}, \\ \Delta\boldsymbol{\varepsilon}_{\sigma,p}^{k} &= \Delta\lambda_{p}\frac{\partial\phi_{M}(\boldsymbol{\sigma}^{k})}{\partial\boldsymbol{\sigma}}. \end{aligned} \tag{6}$$

Here $\Delta\lambda_{p}$ is plastic multiplier and ϕ_{M} is yield surface defined by equivalent von Mises stress and material hardening law.

Material hardening law

In terms of plastic flow potential ϕ_{M}, the equivalent (Mises) stress σ_{M} is to be compared against the material yield stress in each time step of the calculation to check the plasticity criterion. Here yield stress is calculated from the defined hardening law, i.e., a material constitutive law explaining the evolution of yield stress with respect to accumulated plastic strain $\bar{\varepsilon}_{\sigma,p}$ under loading/reloading conditions. The hardening law is typically defined from uni-axial experiments such as, e.g., presented in Poh and Skarajew (1995), which are performed at constant temperature and a controlled stress (or strain) rate, which is high enough to avoid influence of creep. In addition, creep laws are determined separately in classic creep experiments such as, e.g., described in Cowan and Khandelwal (2014). As an alternative, however, a simplified hardening model is also used sometimes where creep strain is in an approximate way implicitly incorporated in the stress-mechanical strain relationship (i.e., $\sigma - \varepsilon_{\sigma,imp-cr}$ relationship). These models are usually derived from transient and steady-state material tests at a variable stress and/or temperature and correspond to a specific range of heating rates.

For the purposes of this paper, two hardening laws were implemented in the prepared Abaqus model:

- the $\sigma - \varepsilon_{\sigma}$ model suggested by Poh (2001, 2014)[1] to be used together with the rate-dependent creep model of Williams-Leir (1983) presented in Section 2.2.4 (limits of the model's applicability: $500℃ \leq T_{\text{steel}} \leq 650℃$, $\varepsilon_{cr} \leq 2\%$); denotation `Poh-WL-model` will be used in the sequel for this model,
- and the rate-independent $\sigma - \varepsilon_{\sigma,imp-cr}$ model suggested by EN 1993-1-2 (2004) (limits of the model's applicability: heating rates between $2\,\mathrm{K/min}$ and $50\,\mathrm{K/min}$)[2]; the denotation will be used further.

The selected material models were implemented into the Abaqus model using the user subroutine UMAT.

2.2.4 Creep strains

For consideration of creep strains the Williams-Leir's creep model is adopted (consult Appendix A), where the rate of equivalent uniaxial creep strain $\bar{\varepsilon}_{cr}$ is given by

$$\dot{\bar{\varepsilon}}_{cr} = b_{1}\coth^{2}(b_{2}\bar{\varepsilon}_{cr}). \tag{7}$$

In Eq. (7) coefficients b_{1} and b_{2} follow the expressions

$$b_{1} = \begin{cases} c_{1}\exp\left(c_{2}\ln\sigma_{M} - \dfrac{c_{5}}{T_{k}}\right), & \sigma_{M} \leq \sigma_{T} \\ c_{6}\exp\left(c_{7}\ln\sigma_{M} - \dfrac{c_{5}}{T_{k}}\right), & \sigma_{M} > \sigma_{T} \end{cases} \tag{8}$$

[1] Other models, e.g., Torić *et al*. (2016a, b) or similar, could be selected here as an alternative.

[2] The EN 1993-1-2 (2004) steel material model was created based on constant-stress coupon tests conducted with a heating rate $10℃/\mathrm{min}$ specifically selected to implicitly include some creep strain (Kirby and Preston 1988).

$$b_2 = \frac{1}{c_3 \sigma_M^{c_4}} \tag{8}$$

where $T_K(K)$ is temperature, σ_T is $15000\,\mathrm{lbf/in^2}$ (103 MPa) and c_1 to c_7 are constants which depend on the type of steel and are given in Williams-Leir (1983).

To solve Eq. (7) we employed forward Euler integration scheme

$$\Delta\bar{\varepsilon}_{cr}^{k} = \dot{\bar{\varepsilon}}_{cr}(\sigma_M^{k-1})\Delta t, \tag{9}$$

where the increment of the creep strain is calculated at the beginning of the step based on equivalent stress from the previous step. Such scheme requires limitation of the size of the time steps to minimize the error. For purposes of this paper the latter was done based on experiences gained in previous validation and verification analyses (see Appendix B).

The multiaxial creep strain increment is obtained based on assumption that direction of creep strains is normal to the plastic potential

$$\Delta\boldsymbol{\varepsilon}_{cr}^{k} = \sqrt{\frac{2}{3}}\Delta\bar{\varepsilon}_{cr}^{k}\frac{\partial\phi_M(\boldsymbol{\sigma}^k)}{\partial\boldsymbol{\sigma}}. \tag{10}$$

2.3 Verification and validation

Prior performing the intended parametric studies, the model presented in Section 2 was extensively validated and verified (see Appendix B). The model was found suitable for further analyses.

2.4 Parametric studies

2.4.1 Aim

Section 2.4 is dedicated to an investigation of possible level of discrepancies between the selected implicit- and the explicit-creep plasticity approach to modelling response of steel beam-girder assemblies with bolted fin-plate connections exposed to fires. The assembly as presented in Sections 2.1 and 2.2 will be used for these purposes.

2.4.2 Description of the studies

Material models

The beam and the connection plate, wherein the highest stress and correspondingly most pronounced creep strains were expected, were defined as to be made of steel with the elastic modulus of 210 GPa and yield strength of 275 MPa. As announced in Section 2.2.3, two material models were applied for description of their material behaviour: the `EC3-model` and the `Poh-WL-model`. Considering the yield strength, the creep coefficients of steel types SS41, A135 and A149 were applied here considering that according to Luecke *et al.* (2005) these steels are steels with US ASTM designation A 36 or European designation S235 and S275.

Heating regime

Different heating regimes were tried out while preparing the study, starting with the original Cardington heating curve. The results at this regime did not reflect in a significant difference between the EC3 and Poh-WL model, however. Searching for such cases further, the Cardington curve was then modified and finally two heating regimes were selected (see Figs. 5 and 6)[3,4] which not only showed on a large difference between the two models but also on the 'unsafe side' of the `EC3-model`. According to heating regime 'I' the assembly was first heated fast up to 550°C. The heating curve applied up to this temperature was similar as the one measured on the beam of the Cardington fire experiment, see Wald *et al.* (2006). After that the assembly was exposed to a slow steady-state heating rate (SSHR) of 2 K/min (analyses I–EC3, I–PWL–SS41, I–PWL–A135, I–PWL–A149). The rate of 2 K/min corresponded to the lower limit at which the $\sigma - \varepsilon_{\sigma,imp-cr}$ model is still applicable in a structural fire analysis. Moreover, a 'steady state' heating rate (SSHR) of 0.9 K/min (heating regime 'II') was also tested in the same manner (analyses II–EC3, II–PWL–SS41, II–PWL–A135, II–PWL–A149). The idea of running all of the analyses once more at 0.9 K/min was to explore possible consequences when the usage of the implicit-creep plasticity approach is improperly stretched outside the allowable limits. Material and heating characteristics of the described analyses are summarised in Table 1. Other characteristics that are not mentioned here explicitly, were taken the same as in Section 2.3 and Appendix B.

Loading of the assembly (utilization factor)

The loadings of the girder and the beam were first selected as $p_{\mathrm{girder}} = 72.9\,\mathrm{kN/m^2}$ and $p_{\mathrm{beam}} = 23.7\,\mathrm{kN/m^2}$, respectively. These selections equalled the room temperature utilization factor[5] of the assembly around 25% with respect to its elastic bearing capacity and 15% with respect to its ultimate plastic capacity (Fig. 2). In addition, other possible utilization factors as mentioned in EN 1993-1-2:2005 (see e.g., Figure 2.1 or Table 4.1 of this standard) were checked as well. The difference between both modelling approaches was found significant for the utilization factors less than 35%, thus, only these results were shown in details in this paper (see Section 3). In general (as shown e.g., in Figure 2.1 of EN 1993-1-2:2005), utilization factors less than 35% are typical for cases when the ratios between the live and the permanent load are greater than 3 and when the combination factor for fire load

[3] In fires of real buildings, similar time-temperature development is often observed within better ventilated regions of the building (i.e., near windows and other openings enabling entrance of fresh cool air from the outside). This is also the reason why such curves often resemble the nominal curve for external fires as proposed in EN 1991-1-2.

[4] Cooling phase of the fire was not considered in this paper. Only cases when the structure collapses already in the heating phase were discussed.

[5] The term utilization factor used here represents the ratio between the effect of actions on the member and the member's resistance, see EN 1993-1-2 (2004), clause 4.2.4(3).

Table 1 Parametric studies: Basic characteristics of the performed analyses

Analysis	Heating regime (SSHR*)	Material model	Creep characteristics, as for steel
I-EC3	I	`EC3-model`	(**)
I-PWL-A135	I	`Poh-WL-model`	A135
I-PWL-A149	I	`Poh-WL-model`	A149
I-PWL-SS41	I	`Poh-WL-model`	SS41
II-EC3	II	`EC3-model`	(**)
II-PWL-A135	II	`Poh-WL-model`	A135
II-PWL-A149	II	`Poh-WL-model`	A149
II-PWL-SS41	II	`Poh-WL-model`	SS41

* Note: SSHR I = 2 K/min, SSHR II = 2 K/min
** Note: Implicit-creep analysis applied

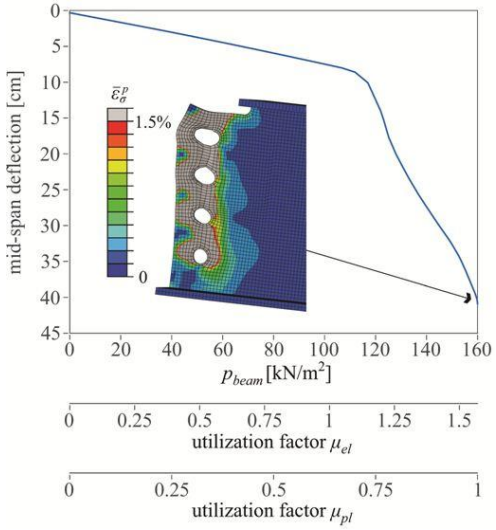

Fig. 2 Parametric studies: load-deflection curve of the selected beam-girder assembly at ambient temperature conditions with denoted elastic and plastic utilization factors and accumulated plastic strains at failure

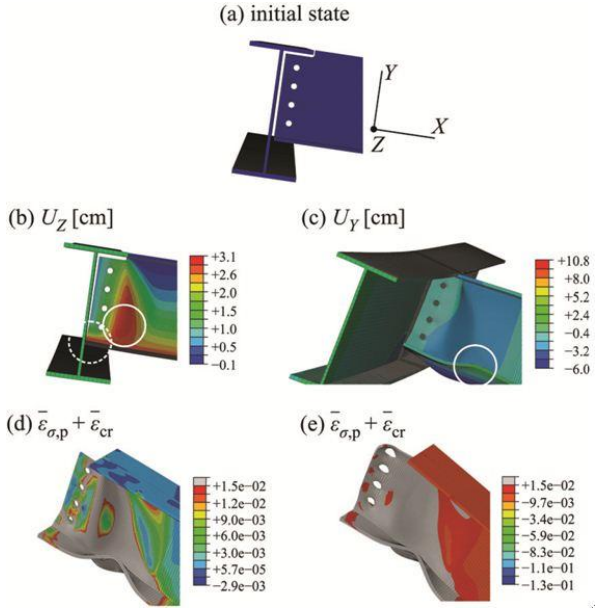

Fig. 3 Typical response of the analysed assembly. The grey areas in figures 'd' and 'e' represent the area with the $\bar{\varepsilon}_{\sigma,p}+\bar{\varepsilon}_{cr} \geq 1.5\%$ with 1.5% corresponding approximately to the limit at which the cumulative plastic strain $\bar{\varepsilon}_{\sigma,p}+\bar{\varepsilon}_{cr}$ progresses at constant stress according to EN 1993-1-2 (2004)

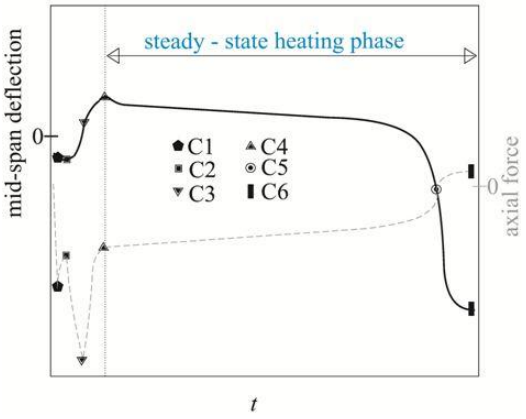

Fig. 4 Parametric studies: typical courses of the graphs of mid-span deflections and axial force of the beam

combination is around 0.2. In the engineering practice, such ratios (greater than 3) are typical for lightweight structures exposed to high value external loads (e.g., wind or snow), e.g., as in typical roof or atrium assemblies. They are less common for the alternative floor assemblies where steel frames are often connected to heavy concrete slabs that increase the dead load of the assembly.

2.4.3 Mechanical response of the assembly and failure time

This section summarizes typical characteristics of the mechanical response of the analysed assembly (Fig. 3 and 4). The failure time as defined in this paper is also explained.

On account of the bolt-induced restraints in thermal deformations of the beam, buckling of the web of the beam is detected first around the bolts (circled area in Fig. 3(b), point C1 in Fig. 4). The second characteristic is a consequence of the combined effect of the mechanical loading (and the consequential deflection of the beam) and the thermal loading (and the corresponding thermal elongations of the beam outside the bolts region); both loadings eventually causing a contact between the bottom flange of the beam and the web of the girder (dashed-circled area in Fig. 3(b), point C2 in Fig. 4). When this contact is established, the effect of the consequentially increased fire-induced compressive axial stresses overcomes the mechanically-induced tensile stresses in the bottom parts of the beam and pushes the beam upwards so that its mid-span deflection decreases. Soon after, buckling of the beam's bottom flange is detected as well (circled region in Fig. 3(c), point C3 in Fig. 4) which causes a reduction of the

previously fast increasing compressive axial force. After the buckling gets more distinct, the reverse in the vertical displacements of the beam is caused as well and the beam starts sagging (C4 in Fig. 4). The final significant characteristic is evolution of larger areas of cumulative (mechanical plus creep) plastic strains within and around the buckled areas of the beam's flange and its web and around the bolts (consequence of stress concentrations around bolt holes). These finally grow together into extensive area of plastic strain localization (grey region in Fig. 3(d)) and cause the previously clamped-like structural system of the beam to move closer to a pinned-like one (point C5 in Fig. 4). This conversion may be seen very clearly from the graph of the beam's mid-span deflections because it is often triggered with a rate of deflection which is higher compared to the rate defined as limiting in standard fire experiments, see EN1363 (2004)

$$\left(\frac{dD}{dt}\right)_{\text{limiting}} = \frac{L^2}{9000\,d}\frac{\text{mm}}{\text{min}}, \tag{11}$$

where L is the clear span of the test specimen (in millimetres) and d is the distance from the extreme fibres of the cold design compression and tension zone of the structural section (also in millimetres). In any case, however, the conversion is seen from the graph of mid-span axial force of the beam, which is now decreased to zero. Past the conversion, the beam might stabilize (regain balance) in a new position and bear the load somewhat longer. Nevertheless, substantial pull forces will now evolve in the connections as a result of the beam's recent large end-rotations that accompanied the conversion and soon (especially because larger plastifications have already evolved previously in these regions) these will cause the beam to fail across the bolted cross-section (see Fig. 3(e) and point C6 in Fig. 4). In this paper, the time of the conversion of the beam (i.e., the time when the beam's axial force is dropped to zero) was, thus, selected as the time of the beam's failure.

3. Results and discussion

This section presents and discusses results of the parametric study. First, the results for when the utilization factor of the assembly with respect to its room temperature elastic bearing capacity was around 25% are shown. Later, some results are also shown for other utilization factors and loading conditions.

Results at utilization factor 25%

Results of the performed parametric studies at utilization factor of the assembly 25% are shown in Figs. 5-7. Figs. 5 and 6 first compare the time evolutions of the mid-span deflection of the beam and the connection rotation for all of the analysed cases. In general, localized plastic zones in

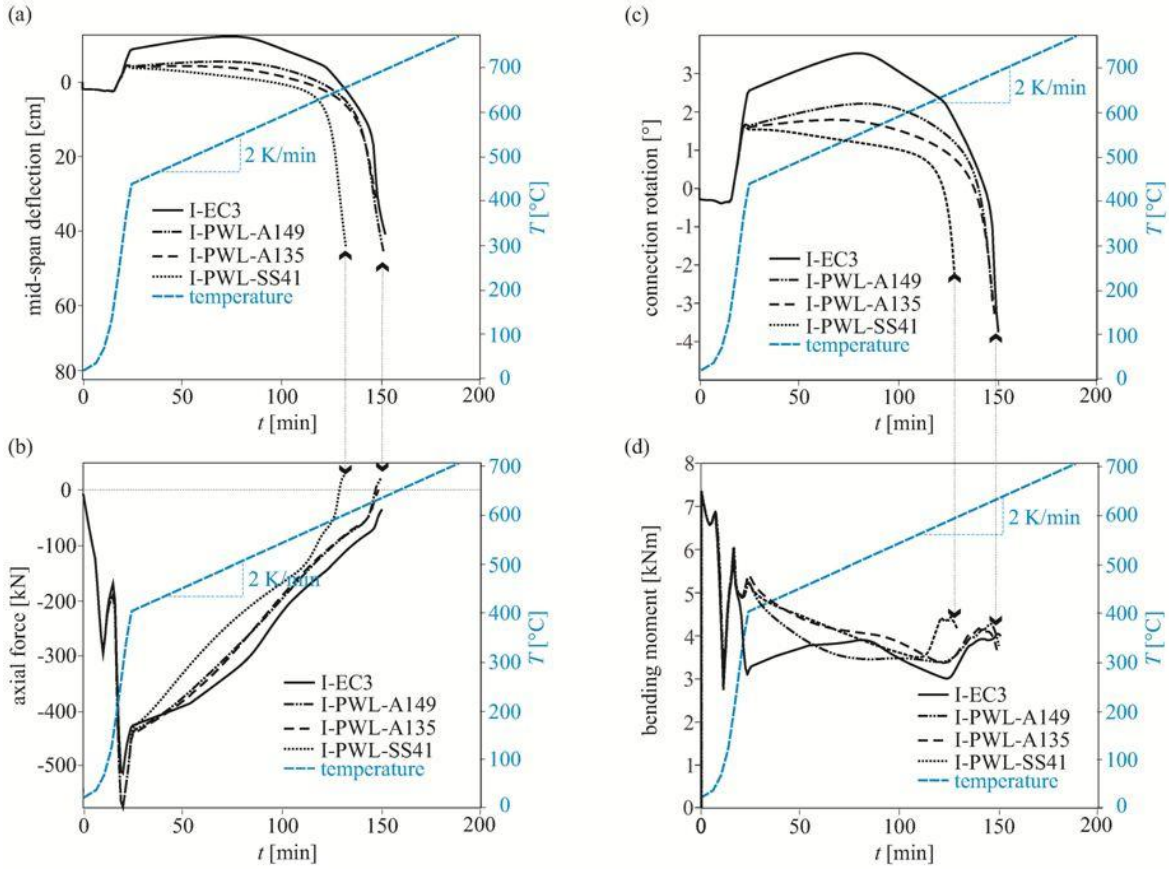

Fig. 5 Parametric studies - main results of analyses type 'I' (SSHR = 2 K/min) for different steel types: (a) mid-span deflection; (b) mid-span axial force; (c) connection rotation; and (d) connection bending moment

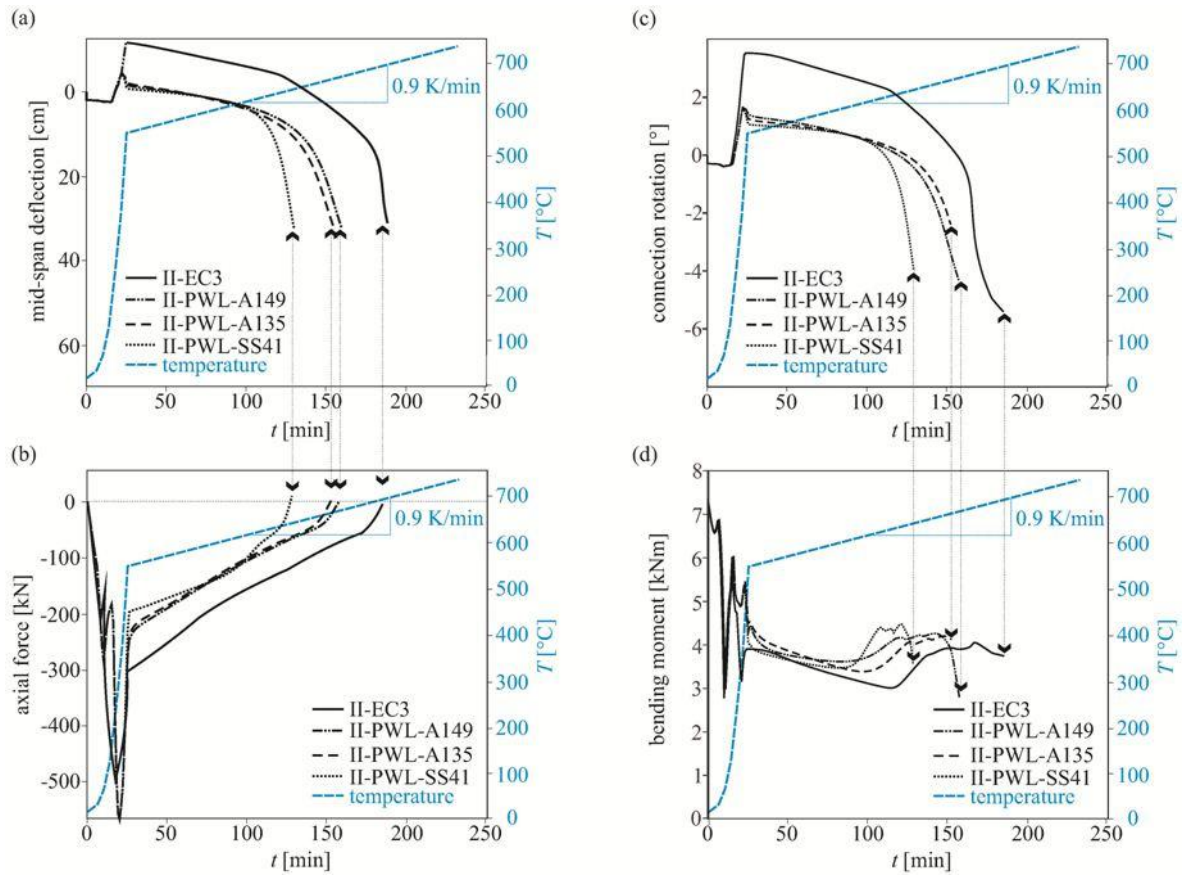

Fig. 6 Parametric studies - main results of analyses type 'II' (SSHR = 0.9 K/min) for different steel types: (a) mid-span deflection; (b) mid-span axial force; (c) connection rotation; and (d) connection bending moment

mid-span and in the connection, together with local instability effects in the connection, form a two node plastic hinge mechanism, therefore the shape of the rotation curves closely resemble the deflection curves. The time evolution of the axial force of the beam is also shown for better detection of the failure time of the beam (see Section 2.4.3 for definition of the failure time), as well as the time evolution of the connection bending moment. In addition, evolution of the beam's temperature is also attached for easier interpretations.

It is interesting to notice that for times before entering the steady-state heating stage in each figure the general course of graphs is similar for the `EC3-model` analysis and all of the `Poh-WL-model` analyses and only deviations in the size of the evolved mid-span deflections are noticed. Since no significant creep is evolved in the structure during this stage[6], these deviations can be contributed to differences in the evolved mechanical strains models. Afterwards, however, the discrepancies are especially on account of the evolved creep. This can be observed in Fig. 7 showing evolution of $\bar{\varepsilon}_{\sigma,p}$ (or $\bar{\varepsilon}_{\sigma,imp-cr,p}$) and $\bar{\varepsilon}_{cr}$ at the start and the end of the steady-state phase for analyses I (SSHR = 2 K/min). It is seen very clearly that while the mechanical strains remain almost the same throughout this phase, the increase in creep strains is substantial. For analyses II ($\mathrm{SSHR} = 0.9\,\mathrm{K/min}$) these conclusions were similar[7]. Furthermore, for $2\,\mathrm{K/min}$ analyses (analyses I) the failure is achieved at approximately the same times (Figs. 5 and 6) and there is no significant difference between the `EC3-model` and the `Poh-WL-model` analyses for most of the explored steels (the exception being steel type SS41). This demonstrates that, when staying within the limits of the `EC3-model` applicability, the implicit creep approach of EC3 is accurate enough for the majority of the explored cases. More differences in the time of failure are, although, observed for analyses type II ($0.9\,\mathrm{K/min}$ analyses) where all of the failure times calculated by the `Poh-WL-model` are (even substantially) shorter than the ones calculated by the `EC3-model`. It is, thus, obvious that when the applicability of the `EC3-model` is improperly stretched to heating rates less than $2\,\mathrm{K/min}$, a substantial error should be expected.

Table 2 summarizes the calculated failure times and temperatures calculated in the performed explicit-creep plasticity analyses and compares them to the corresponding

[6] To see this, compare the graphs of the `Poh-WL-model` analyses in each figure and notice that they coincide almost completely for earlier times (up to $T = 550$°C, i.e., regardless of what creep coefficients were applied.

[7] The distributions of $\bar{\varepsilon}_{\sigma,p}$ (or $\bar{\varepsilon}_{\sigma,imp-cr,p}$) and $\bar{\varepsilon}_{cr}$ across the connection were similar but the $\bar{\varepsilon}_{cr}$ were about five times larger.

Table 2 Failure times and temperatures of the performed analyses. Denotation $t_{\mathrm{f,EC3}}$ denotes the failure time of the corresponding EC3 analysis (i.e. I–EC3 or II–EC3 analysis)

Analysis acronym	t_{failure} [min]	T_{failure} [°C]	$\frac{t_{\mathrm{failure}} - t_{\mathrm{f,EC3}}}{t_{\mathrm{f,EC3}}}$
I-PWL-SS41	128	596	15.2 %
I-PWL-A135	148	632	2.0 %
I-PWL-A149	147	629	2.6 %
I-EC3	151	638	-
II-PWL-SS41	127	640	31.0 %
II-PWL-A135	152	662	17.4 %
II-PWL-A149	157	668	14.7 %
II-EC3	184	692	-

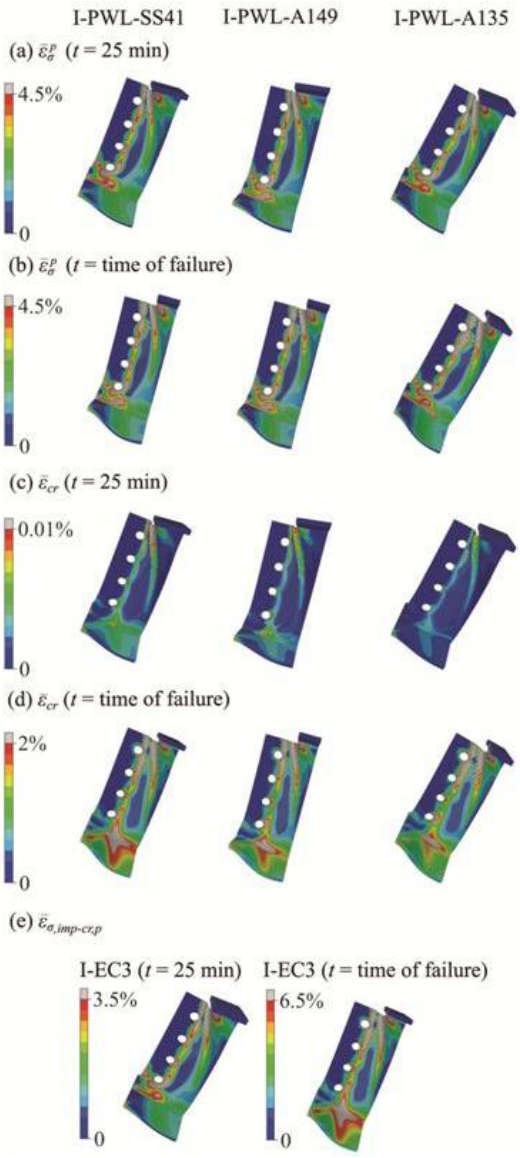

Fig. 7 Parametric studies (analyses 'I'): Mechanical and creep strains evolved in the beam along the beam-girder connection at the start of the '2 K/min' phase $t = 25$ min and at the time of failure

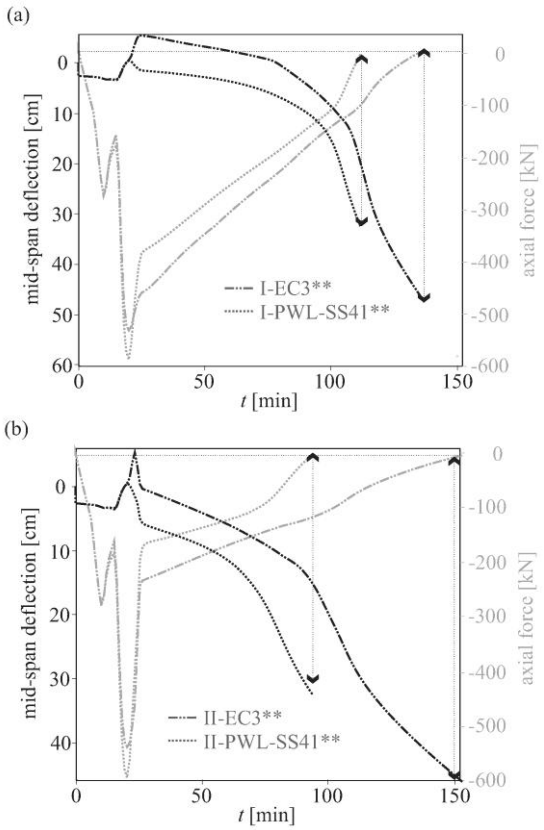

Fig. 8 Mid-span deflections and axial force for analyses type 'I' (SSHR = 2 K/min) and 'II' (SSHR = 0.9 K/min) at somewhat changed loading conditions

failure times and temperatures of the implicit-creep analyses.

Results at other geometry and loading

Fig. 8 and Table 3 show some of the results for cases when p_{beam} was increased to 35.6 kN/m^2 (i.e., the aforementioned utilization factors with respect to the elastic and ultimate plastic bearing capacity of the assembly at time $t = 0$ were increased to 35% and 25%, respectively). The figure leads to conclusions, which are similar to those of Figs. 5 and 6. For even higher utilization factors, however, the `EC3-model` in general produced failure times, which were similar or somewhat shorter as when using `Poh-WL-model`. Further studies (in progress) will be necessary to pin-point whether this is just a specificity of the selected structural case under analysis (its geometry, heating regime etc.), selected materials and the corresponding material models (i.e., Williams-Leir models for SS41, A135 and A149) or other.

Furthermore, some analyses were also performed to check the results at other geometric and/or heating conditions. Fig. 9 and Table 3, for example, demonstrate results of analyses with SSHR = 0.9 K/min but with a somewhat changed geometry of the beam (thickness of the web of the beam is reduced to 4.5 mm) and with somewhat modified 'pre-steady-state' heating conditions (the assembly is heated somewhat faster as before and to a higher temperature in the 'pre-steady-state' phase). As can

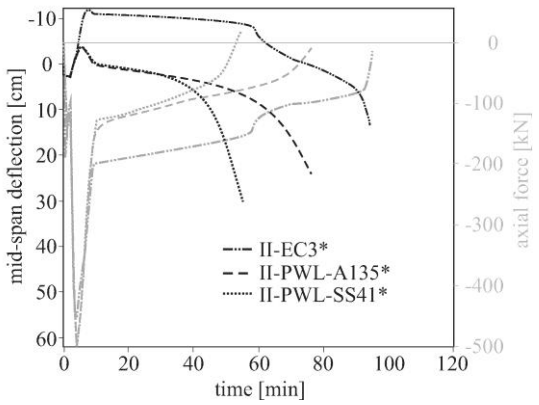

Fig. 9 Mid-span deflections and axial force for analyses type 'II' (SSHR $= 0.9\,\mathrm{K/min}$) with somewhat modified 'pre-steady-state' heating conditions and slightly changed geometrical data

Table 3 Failure times and temperatures of additional analyses

Analysis acronym	t_{failure} [min]	T_{failure} [°C]	$\frac{t_{\mathrm{failure}} - t_{\mathrm{f,EC3}}}{t_{\mathrm{f,EC3}}}$
I-PWL-SS41**	111	683	18.4 %
I-EC3**	136	737	-
II-PWL-SS41**	93	613	38 %
II-EC3**	150	663	-
II-PWL-SS41*	53	640	43.6 %
II-PWL-A135*	77	661	18.1 %
II-EC3*	94	677	-

*Note: analyses with somewhat modified 'pre-steady-state' heating conditions and slightly changed geometrical data.
** Note: analyses with somewhat changed loading conditions

be expected, the absolute values of failure times obtained here are shorter than those of Figs. 5 and 6 but the relative deviations between them are again similar.

Special comments

The discrepancies between results of the implicit-creep plasticity and the alternative explicit-creep plasticity approach as demonstrated in this paper should be considered as being 'as shown or higher' for the reasons explained in Appendix C.

4. Conclusions

This paper investigated the effects of creep on fire response of classic steel beam-girder assemblies exposed to fires. The results are applicable for the assemblies with the fin-plate connections, which are designed such that the bolts have sufficient capacity and that failure mechanism occurs in the connected plates.

The study was done by means of a specially designed numerical model which was suitably validated and verified. Possible discrepancies between the selected implicit- and explicit-creep plasticity modelling approaches were also explored. For the explicit-creep analyses, the combination of $\sigma - \varepsilon_{\sigma}$ model of Poh and the creep model of Williams-Leir was applied (`Poh-WL-model`). Creep coefficients of different steels were tried out, i.e., coefficients for steels SS41, A135 and A149 representing steels similar to steels with US ASTM designation A 36 or European designation S235 and S275. In the 'implicit-creep' plastic analyses the $\sigma - \varepsilon_{\sigma,imp-cr}$ model suggested by EN 1993-1-2 was used (`EC3-model`). The main analyses were performed at the mechanical loading of such a level that the utilization factor of the beam was 25 %. In addition, they were performed at two different heating regimes, i.e., one with the steady-state ('post-flashover') heating rate of $0.9\,\mathrm{K/min}$ ($\mathrm{SSHR} = 0.9\,\mathrm{K/min}$) and one with $\mathrm{SSHR} = 2\,\mathrm{K/min}$. Rate of $2\mathrm{K/min}$ here corresponded to the lower limit at which the `EC3-model` is declared to be still applicable for a structural fire analysis, rate of $0.9\,\mathrm{K/min}$ was a rate outside (below) this limit. The paper finally showed that, when the usage of `EC3-model` is stretched to fire scenarios with heating rates slower than the allowed lower limit what is often observed in the engineering practice, the failure times calculated by this improperly applied approach can be up to 38% longer compared to the correctly applied `Poh-WL-model` approach. Within the limits, however the discrepancies between both approaches were found negligible for majority of the explored cases with the exception of the results for SS41 steel assemblies. For the latter, the calculated failure times were up to 19% shorter according to `Poh-WL-model` approach.

Furthermore, some analyses were also performed to check the results at some other geometric conditions but similar conclusions were drawn. In addition, some calculations were prepared with applied higher mechanical loads, i.e., higher utilization factors of the beam. For the utilization factors up to 35% similar conclusions were drawn once more. However, when the utilization factors became even higher, the failure times calculated by the `EC3-model` approach became similar or somewhat shorter as compared to the `Poh-WL-model` approach. More future investigation is encouraged to support the findings of this paper with a special recommendation on further development of experimentally-based creep models and their extensive validations including validations on largescale structural assemblies.

Acknowledgments

The work of J. Kolšek was funded by the Slovenian Research Agency (grant nubmer Z7 7677). The work of M. Kramar and P. Češarek is supported by the Slovenian Research Agency, research core fundings No. P2-0273 and No. P2-0260, respectively.

References

ABAQUS (2016), Documentation, DS-Simulia; Providence, RI,

USA, AISC.
Anderberg, Y. (1988), "Modelling steel behaviour", *Fire Saf. J.*, **13**, 17-26.
EN 1993-1-2 (2004), Eurocode 3: Design of Steel Structures. Part 1.2: General rules - Structural fire design, European Committee for Standardization; Brussels, Belgium.
EN 1363-1 (2012), Fire resistance tests, Part 1: General requirements, European Committee for Standardization; Brussels, Belgium.
Chan, Y.K., Iu, C.K., Chan, S.L. and Albermani, F.G. (2010), "Performance-based structural fire design of steel frames using conventional computer software", *Steel Compos. Struct., Int. J.*, **10(**3), 207-222.
Cowan, M. and Khandelwal, K. (2014), "Modeling of high temperature creep in ASTM A992 structural steels", *Eng. Struct.*, **80**, 426-434.
Harmathy, T.Z. (1967), "A comprehensive creep model", *J. Basic Eng.*, **89**, 496-502.
Huang, Z.F., Tan, K.H. and Ting, S.K. (2006), "Heating rate and boundary restraint effects on fire resistance of steel columns with creep", *Eng. Struct.*, **28**, 805-817.
Kirby, B.R. (1995), "The behavior of high-strength grade 8.8 bolts in fire", *J. Constr. Steel. Res.*, **33**, 3-38.
Kirby, B.R. and Preston, R.R. (1988), "High temperature properties of hot-rolled, structural steels for use in fire engineering design studies", *Fire Saf. J.*, **13**, 27-37.
Kodur, V.K.R. and Dwaikat, M.M.S. (2010), "Effect of high temperature creep on the fire response of restrained steel beams", *Mater. Struct.*, **43**, 1327-1341.
Kodur, V., Dwaikat, M. and Fike, R. (2010), "High-temperature properties of steel for fire resistance modeling of structures", *J. Mater. Civ. Eng.*, **22**, 423-434.
Kolšek, J. and Češarek, P. (2015), "Performance-based fire modeling of intumescent painted steel structures and comparison to EC3", *J. Constr. Steel. Res.*, **104**, 91-103.
Kolšek, J., Planinc, I., Saje, M. and Hozjan, T. (2013), "The fire analysis of a steel-concrete side-plated beam", *Finite Elem. Anal. Des.*, **74**, 93-110.
Kolšek, J., Planinc, I., Saje, M. and Hozjan, T. (2014), "A fully generalised approach to modelling fire response of steel-RC composite structures", *Int. J. Nonlin. Mech.*, **67**, 382-393.
Li, G.Q. and Zhang, C. (2012), "Creep effect on buckling of axially restrained steel columns in real fires", *J. Constr. Steel Res.*, **71**, 182-188.
Luecke, W.E., McColskey, J.D., McCowan, C.N., Banovic, S.W., Fields, R.J., Foecke, T., Siewert, T.A. and Gayle, F.W. (2005), "NIST NCSTAR 1-3D: Federal Building and Fire Safety Investigation of the World Trade Center Disaster: Mechanical Properties of Structural Steel", Research Report No. NIST NCSTAR 1-3D; NIST National Institute of Standards and Technology, Technology Administration, U.S. Department of Commerce, U.S. Government Printing Office, Washington, DC, USA.
Poh, K.W. (2001), "Stress-strain-temperature relationship for structural steel", *J. Mater. Civil Eng.*, **13**, 371-379.
Poh, K.W. (2014), "Erratum for 'Stress-strain temperature relationship for structural steel'", *J. Mater. Civil. Eng.*, **26**, 388-389.
Poh, K.W. and Skarajew, M. (1995), "Elevated temperature tensile testing of grade 300PLUSe hot rolled structural steel", Rep. No. BHPR/SM/R/007; BHP Research Melbourne Labs, Melbourne, Australia.
Rubert, A. and Schaumann, P. (1985), "Temperaturabhängige Werkstoffeigenschaften von Baustahl bei Brandbeanspruchung", *Stahlbau*, **3**, 81-86.
Simo, J.C. and Hughes, T.J.R. (1998), *Computational Inelasticity*, Springer-Verlag, New York, NY, USA.
Torić, N. and Burgess, I.W. (2016), "A unified rheological model for modelling steel behaviour in fire conditions", *J. Constr. Steel Res.*, **127**, 221-230.
Toric, N., Harapin, A. and Boko, I. (2013), "Experimental verification of a newly developed implicit creep model for steel structures exposed to fire", *Eng. Struct.*, **57**, 116-124.
Toric, N., Harapin, A. and Boko, I. (2015), "Modelling of the influence of creep strains on the fire response of stationary heated steel members", *J. Struct. Fire Eng.*, **6**, 155-176.
Torić, N., Sun, R.R. and Burgess, I.W. (2016a), "Creep-free fire analysis of steel structures with Eurocode 3 material model", *J. Struct. Fire Eng.*, **7**, 234-248.
Torić, N., Sun, R.R. and Burgess, I.W. (2016b), "Development of a creep-free stress-strain law for fire analysis of steel structures", *Fire. Mater.*, **40**, 896-912.
Torić, N., Brnic, J., Boko, I., Brcic, M., Burgess, I.W. and Glavinic, I.U. (2017), "Development of a high temperature material model for grade S275JR steel in fire", *J. Constr. Steel Res.*, **137**, 161-168.
Wald, F., da Silva, L.S., Moore, D.B., Lennon, T., Chladna, M., Santiago, A., Beneš, M. and Borges, L. (2006), "Experimental behaviour of a steel structure under natural fire", *Fire Saf. J.*, **41**, 509-522.
Williams-Leir, G. (1983), "Creep of structural steel in fire: Analytical expressions", *Fire Mater.*, **7**, 73-78.
Witteveen, J. and Twilt, L. (1975), "Behaviour of steel columns under fire action", *International Colloquium on Column Strength*, Paris, Volume 23.
Yang, K.C. and Yua, Z.H. (2013), "Experimental research on the creep buckling of fire-resistant steel columns at elevated temperature", *Steel Compos. Struct., Int. J.*, **15**(2), 163-173.

CC

Appendix A

A. Discussion on the selected creep model

Under constant temperature and stress, creep strains of steel in general exhibit three separate phases: (i) primary phase (where $d^2\varepsilon_{cr}/dt^2 < 0$), (ii) secondary phase (where $d^2\varepsilon_{cr}/dt^2 \approx 0$ i.e., the strain rate becomes near constant), and (iii) tertiary phase (where $d^2\varepsilon_{cr}/dt^2 > 0$ and the strain rate increases exponentially with time). Proposals of creep models including all three phases, however, are rare. This is probably because waiting that the tertiary stage is reached in a material creep experiment elongates the test significantly and increases its costs. In addition, see e.g., Williams-Leir (1983), historically it was often considered that strains unacceptable in the steel of a building will develop no later than during the secondary stage (not necessarily true as pointed out in this paper). Moreover, even when simplified with exclusion of the tertiary phase, however, derivation of a creep model is still costly for another two important reasons: (i) different types of steel often exhibit very different creep behaviours, thus, each type of steel needs to be tested separately, (ii) tests based on which creep models are derived and validated (steady-state and transient tests) should reflect realistic engineering conditions to the broadest range possible.

Among the creep models, found by the authors, e.g., the models of Harmathy (1967), Williams-Leir (1983), Kodur and Dwaikat (2010), Kodur *et al*. (2010), Torić and Burgess (2016), Torić *et al*. (2017), Cowan and Khandelwal (2014) etc., the model of Williams-Leir (1983) for A135, SS41, A149 and SM50 steels, which are steels similar to steel with US ASTM designation A 36 or European designation S235 and S275 as reported in Luecke *et al*. (2005), was selected for further analyses. This model includes primary as well as secondary creep phases. Its coefficients, as explained in Williams-Leir (1983), were derived on experimental data at constant temperature and stress. However, the functionality of the model was also checked for transient conditions, more precisely for conditions of the experiments of Witteven and Twilt (1975). Moreover, additional validations of this creep model (combined with the mechanical model of Poh) were also done by the authors of the present paper (please, see Appendix B).

Regardless of their choice, the authors wish to emphasize that prioritizing the suggestions of Williams-Leir's over other available creep models was not one of their intentions. Other models, e.g., as listed above, could also be used equally and will be tried out in future work of the authors. The purpose of this paper was simply to demonstrate possible discrepancies between the implicit- and explicit-creep plasticity modelling approaches on the basis of one of the creep models as used today and, if a potential significant discrepancies would be shown, to encourage further research in this field.

Appendix B

B. Discussion on the selected creep model

B.1 Verification of the UMAT algorithm

To verify the prepared UMAT algorithm a comparison of its results to the results of another similar-purpose computational code was performed. The FEA code CompositeBeam presented in Kolšek *et al*. (2013, 2014) was selected for these purposes which is a code that can be used for analyses of one-or multi-layered steel and/or concrete beam-like structures.

A simply supported IPE80 beam made of steel ($E_{20°C} = 21200\,\mathrm{kN/cm^2}$, $\sigma_{20°C} = 33.5\,\mathrm{kN/cm^2}$) and of 114 cm length was analysed. This was loaded in its mid-span by a concentrated load 8 kN. The beam was subjected to a heating rate imposed as a simple temperature boundary condition on all beam surfaces. This was selected in the way that noticeable creep deformations would evolve in the beam what enhanced efficiency of the intended verification (i.e., within first 6 minutes the beam was heated linearly from $20℃$ to $470℃$, after that a slower linear heating regime was imposed until $700℃$ was achieved in the 120th minute). The beam was analysed using: (i) the code CompositeBeam and (ii) using a separate model of such a beam which was prepared in Abaqus by implementing the same modelling techniques as explained in Sections 2.1 and 2.2. For each model, two material submodels were tried out: (i) Poh's model proposed in Poh (2001) and Poh (2014), (ii) Poh's model combined with the creep model of Williams-Leir (1983) for steel type SM50. The results of the verification are shown in Fig. B1 and demonstrate a good agreement between the compared models.

B.2 Validation of material models

For validation of the selected material models a comparison against experimental data was done. The work of Rubert and Schaumann (1985) was used, who tested simply supported IPE80 beams of length 114 cm under simultaneous mechanical and thermal loading. The beams

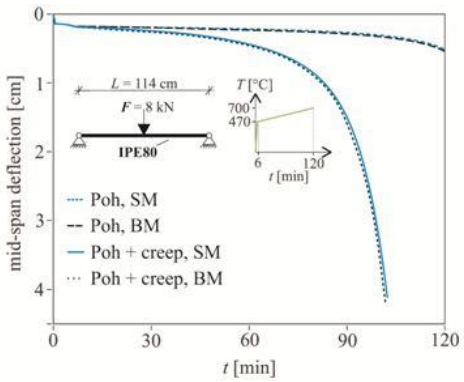

Fig. B1 Verification of the UMAT algorithm: mid-span deflections of the IPE80 beam. Denotations 'SM' and 'BM' refer to '3D solid FE model' and '1D beam FE model', respectively

were tested under different levels of concentrated mid-span loading representing 0.20, 0.50, 0.70, 0.85 of the beam's ultimate load carrying capacity at room temperature. In addition, they were tested at three different heating rates, i.e., 2.67 K/min, 5.33 K/min and 32 K/min. The 0.2 and 0.5 loading levels and the 2.67 K/min and 5.33 K/min heating regimes were selected for the validation analysis in this paper corresponding to slow heating rates and low loading levels applied later in the parametric studies. For the elastic modulus at room temperature the value $E_{20°C} = 19200\ \mathrm{kN/cm^2}$ was used as suggested in Kirby and Preston (1988). The yield strength was taken from the measurements of Rubert and Schaumann (1985), i.e., as $\sigma_{20°C} = 39.9\ \mathrm{kN/cm^2}$. In addition to the `Poh-WL-model` with the creep coefficients for steel type SM50, the simulation was also performed using the `EC3-model`. Note that, according to Luecke *et al*. (2005), SM50 is the most similar type of steel compared to the one used in the Ruber-Schaumann's experiments. The results of the analyses are shown in Fig. B2.

As seen from this figure, all of the tested models recreate the experiments well especially for slow and medium heating rate conditions. For fast heating conditions the discrepancies between the numerical and the experimental results are somewhat higher but seem close enough for engineering applications. Furthermore, considering `EC3-model`, the results show that the preciseness of this implicit-creep model is similar to the applied `Poh-WL-model` (i.e., the failure occurs at somewhat later times as observed in the experiments). Nevertheless, this might be reduced for more complex structures as demonstrated in Section 3 of the paper.

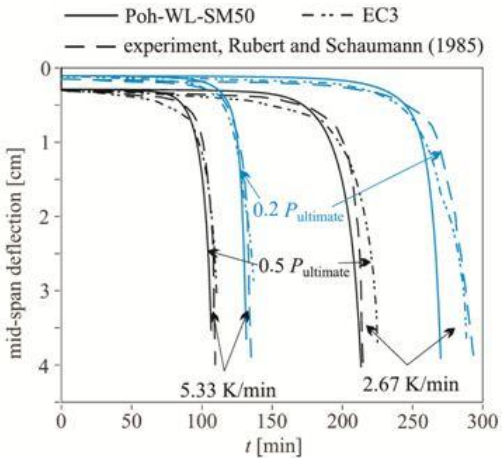

Fig. B2 Verification of the UMAT algorithm: mid-span deflections of the IPE80 beam. Denotations 'SM' and 'BM' refer to '3D solid FE model' and '1D beam FE model', respectively

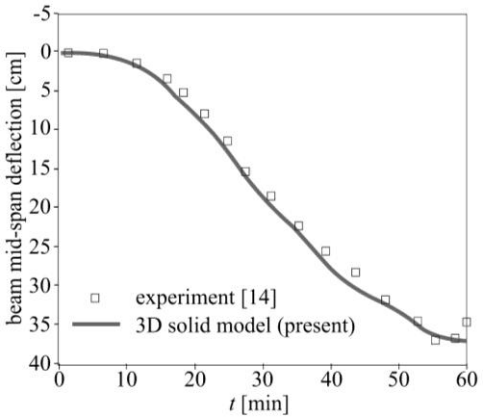

Fig. B3 Cardington experiment - mid-span deflections of the beam

B.3 Validation of the beam-girder model

After gaining confidence in the selected material models and the prepared UMAT subroutine, validation of the modelling techniques used for preparation of the geometrical parts of the beam-girder model (e.g., contact interactions etc.) was also necessary. This model was therefore used to simulate the response of the steel-frame floor subassembly tested in the well-known fire experiment performed in 2003 in Cardington reported in Wald *et al.* (2006). The Cardington experiment was already simulated before by the authors, i.e., see Kolšek and Češarek (2015), however, by implementing the implicit-creep steel model of EN 1993-1-2 (2004) only. For purposes of this paper, this Eurocode's model was replaced by: (i) material model of Kirby (1995) for the bolts, (ii) `Poh-WL-model` with A135-steel characteristics for the shear plate and the beam which were made of steel type S275 according to Wald *et al.* (2006), (iii) `Poh-WL-model` with SM50-steel characteristics for the girder made of steel S355. Data on other characteristics of the model, such as geometric, loading, and contact, can be observed in Kolšek and Češarek (2015, Sec. 2.4).

Fig. B3 shows the final results of the validation and proves a good agreement of the present numerical results with the corresponding experimental observations.

Appendix C

C. Interpretation of presented results

As described in Williams-Leir (1983), the usage of the Williams-Leir's creep model can only be considered reliable for temperatures between 500°C and 650°C and for creep deformations up to 2%. The meaning of these limitations for the results shown in this paper is discussed below.

In all analyses the Williams-Leir's expressions were applied also for creep deformations greater than 2%. This means that the time rate of creep deformations after exceeding 2% was considered to be the same as right before reaching this limit and was considered to stay this way indefinitely although in reality the rate should accelerate at some point and enter the tertiary stage. Consequently, in all analyses the calculated creep deformations may be more or less underestimated for times greater then the time at which first $\bar{\varepsilon}_{cr} \geq 2\%$ were evolved. In addition, at these times the overall deflections of the beam and their time rates are likely underestimated as well. It should be, thus, noticed with a special concern that, where considerable discrepancies between the `EC3-model` and the `Poh-WL-model` were discovered in this paper, these discrepancies could be even higher when a precise (i.e., extended suitably for higher levels of $\bar{\varepsilon}_{cr}$) creep model was used.

Furthermore, in the analyses of this paper, the Williams-Leir's expressions were implemented regardless of the actual maximum steel temperature. This seemed problematic initially because in some analyses the failure time of the beam was exceeded slightly above 650°C (but below 700°C). This raised a question regarding the reliability of the analyses' conclusions. To refute the doubts, however, the results of the performed analyses (i.e., analyses in which the Williams-Leir's model was applied also for temperatures above 650°C) were compared against the results of additional comparative analyses. In these the Williams-Leir's model was applied for temperatures up to 650°C, but for higher temperatures an assumption was applied on the rate of creep strains at 700°C being approximately 100 times higher as compared to the rate at 600°[8]. An example of such comparative analysis is shown in Fig. C1.

The comparison showed that the failure times were somewhat longer in the former case (analysis II-PWL-A135 in Fig. C1). This confirms that in reality (i.e., when the Williams-Leir's model was stretched to temperatures above 650° correctly, that is based on suitably extended experiments and numerical fitting analyses) the beam would most probably fail even slightly sooner as demonstrated in this paper and the difference between the analysed modelling approaches would be even slightly higher.

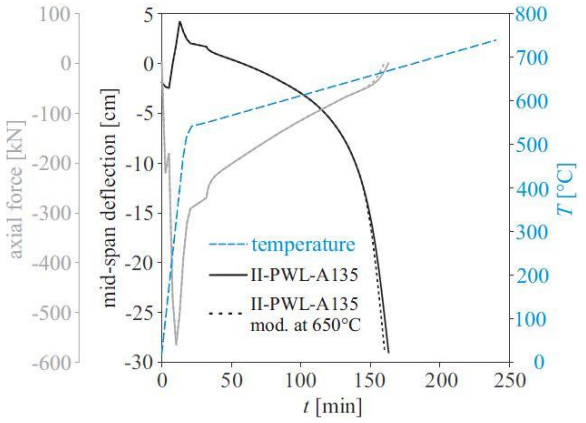

Fig. C1 Comparison between results of analysis IIPWL-A135 calculated with and without modification for temperatures above 650°C (dashed and solid line, respectively)

[8] This approximation was drawn from conclusions of recent experiments of Cowan and Khandelwal (2014).